Automated high-throughput cell microsurgery on-chip†

Kwanghun Chung and Hang Lu*

Received 2nd June 2009, Accepted 11th August 2009
First published as an Advance Article on the web 19th August 2009
DOI: 10.1039/b910703g

Laser cell kill is an established tool for studying cells' roles during development and behavior, but its use has been limited due to the manual and low-throughput nature. We demonstrate here a technique combining multiplexing microfluidic manipulation of *Caenorhabditis elegans* and software for image processing and automation, allowing for high-throughput cell ablations.

In development and neuroscience, it is often important to investigate the roles of individual cells in the tissues and organs of interest. For instance, a fundamental question in neuroscience is how cells in a neural circuit and their connectivity to other cells contribute to the behavior of the organism. Small model organisms such as *Caenorhabditis elegans* (*C. elegans*) are often used for such research, in part because of the well-known anatomy, ease of genetics, and its transparency, which allows for techniques such as cell-specific expression of reporters and laser microdissections.[1–5] In behavioral studies, individual neurons are often ablated by a focused laser beam and animals' behavior changes are examined to infer the function of neurons.[3,6] Although powerful due to its specificity as opposed to genetic ablation,[7] laser ablation has drawbacks in that the difficulty of performing ablation significantly limits the throughput and also introduces large sample-to-sample variation.[5] For example, successful ablation typically occurs at a rate of a few animals per hour. To ablate hundreds of worms required for many population behavior assays would take many hours; for an organism whose lifespan is short, manual ablation typically cannot deliver large numbers of age-synchronized animals. As the number of neurons required to be ablated increases, both the success rate and the throughput suffer. Because the ablated animals often show subtle abnormalities and assays are inherently noisy, many animals are required in order to identify the phenotypical changes reliably. The low-throughput and difficult-to-use nature of the laser ablation limits its use and the pace of discovery, especially in combination with methods requiring large numbers of animals (*e.g.* behavior and RNAi).

To overcome this limitation, we designed and automated an integrated microfluidic system and demonstrated a technique for performing high-throughput cell microsurgery. While several previously developed devices have demonstrated manual handling and axon cutting of *C. elegans* in microfluidic devices,[8–10] automation and high throughput have not been demonstrated. Our method, in contrast, offers automated on-chip animal handling, where age-synchronized animals can be processed in parallel to achieve high-throughput. To ensure successful ablation, our device also uses an immobilization scheme to stop both body movement and pharyngeal pumping of the animal,[11] which is critical for aiming at and ablating multiple cells in a single animal. We use automated image analysis and control of laser ablation, which not only further increases throughput but also allows uniform treatment of animals, thereby reducing experimental noise.

The microfluidic device is optimized for automated operation and has several unique features to maximize throughput (Fig. 1 and Supplementary Video 1†). It is capable of processing multiple worms in parallel without substantially increasing the complexity of the control requirements. It has two sets of worm loading channels that operate in parallel, allowing worm-loading and -exiting at one set, while simultaneously performing imaging and laser ablation in the other set. L1 worms are directed to the loading channels by constant pressure driven flow (~5 psi), and are positioned by restriction structures in the loading/ablation channels (Fig. 1b and Supplementary Video 1†). The loading channels have cross-sectional dimensions similar in size to the cross-sectional diameter (~14 μm) of the L1 worm and length similar to the length (~190 μm) of the worm (Fig. 1b, Supplementary Methods and Materials†). Therefore, the presence of a worm in the loading channel not only increases resistance of the channel and divert worms upstream towards the empty channel,[8] but also physically prevents another worm from loading (Fig. 1b). This passive mechanism reduces the complexity of the control system and enables higher throughput. Once the presence of a worm in the loading channel is determined by the average pixel intensity of a frame from the camera,[11] the loading regulator and resistance regulator are closed (Fig. 1d, f) to further increase the hydrodynamic resistance and thereby reduce buffer flow that can cause movement of the loaded worm. To unload the worm, the restriction valve is open while the loading regulator is closed, which assures releasing of the single processed worm (Fig. 1e and Supplementary Video 1†). The time required for the loading/unloading process varies depending on the density of the worm suspension and variability in worm size: smaller worms experience lower friction during loading/unloading steps, and as a result the process is faster. The parallel processing of worms, however, significantly increases throughput (~50% compared to a single loading channel device) because the time required for the loading/unloading process does not contribute to the effective processing time.

For automated laser ablation, it is crucial that worms remain completely still for the duration of imaging and targeting of the neurons and firing the laser, because any movement or drift can cause inaccurate targeting of the neurons. Body movement and pharyngeal pumping are sources of such movements. We use cooling to immobilize worms; it has several important advantages over other immobilization techniques for automated cell laser kill.[8–12] First, cooling is the only method to stop activity of the pharynx besides using anesthetics. This is particularly important because many sensory and

School of Chemical & Biomolecular Engineering, Georgia Institute of Technology, Atlanta, GA, USA. E-mail: hang.lu@gatech.edu; Tel: +1-404-894-8473

† Electronic supplementary information (ESI) available: Supplementary Methods and Materials, Supplementary Video 1. See DOI: 10.1039/b910703g

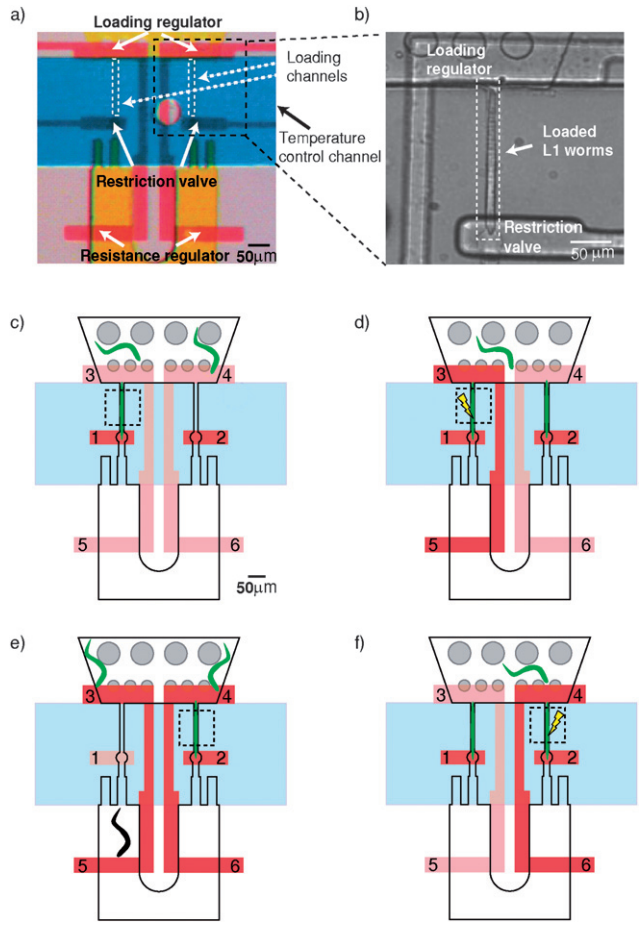

Fig. 1 Microdevice and its operation. (a–b) Optical micrographs of the device. a) Dye-filled image of the device showing active components: sample channel (yellow), valve channel (red), and temperature-control channel (blue). b) A loaded worm in the loading channel. (c–f) Schematic diagrams summarizing the valve control sequence of the device. Valve 1,2: positioning valves, Valve 3,4: loading regulators, Valve 5,6: resistance regulators. The loading- and the resistance-regulator for each loading channel are actuated by a single control channel. Blue, cooling channel; light red, valve in open position; dark red, valves in partially closed position; green worms, animals before ablation; black worms, animals after ablation; dashed square, field of view of the camera. c) Both positioning valves are partially closed for loading. d) To perform laser ablation in the left loading channel, Valve 3 and 5 are partially closed to minimize flow through the left loading channel while Valve 4 and 6 are open to load a worm in the right loading channel. e) After laser ablation of the worm loaded in the left loading channel, the positioning Valve 1 is open to release the ablated worm. The loading regulator (Valve 3) remains closed to prevent non-ablated worms in upstream from exiting. Meanwhile, the x-y-z stage moves to the right loading channel to process a loaded worm. f) The animal in the right loading channel is ablated while another worm is loaded in the left loading channel.

interneurons of interest are near the pharynx. Second, cooling does not cause deformation of the animal's body, which may change the relative anatomical position of the neurons. Therefore, internal anatomical information of cells can be used for image processing algorithms to distinguish target cells from other cells or autofluorescent fat granules in the intestine (Fig. 2). Third, immobilization by cooling is instantaneous and reversible, which allows rapid manipulation of worms.

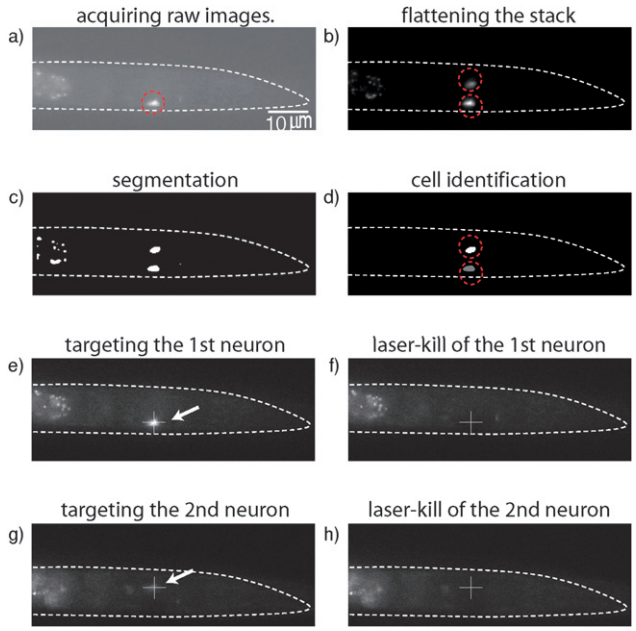

Fig. 2 Process of the automated image processing (a–d) and laser ablation (e–h). a) One frame from the z-stack fluorescent image showing the in-focus neuron (red circle). b) Flattened z-stack image showing two neurons (red circle). c) Thresholded image showing the two neurons and fat granules. d) Processed image showing identified neurons with the fat granules automatically removed. e) Moving the target neuron to the laser focal point. The fluorescent image is taken at the focal plane of the target neuron, and the cross represents the laser position. f) After laser firing: the target neuron is no longer visible in fluorescent image. g) Before laser firing on the second neuron. h) After laser firing on the second neuron.

To ablate neurons expressing green fluorescence protein (GFP) automatically, we use image processing guided by heuristics such as anatomical information of the neurons in the worms. Once the worm is immobilized in the loading channel, sparse z-stack (2-μm steps) is acquired with 100× oil-immersion objective (NA = 1.4) using an EM CCD camera (Fig. 2a). The z-stack is then flattened by computing the standard deviation of pixel in the x-y plane along the z-direction (Fig. 2b). A threshold is subsequently applied to the processed image to identify all local maxima, which include the target neurons and at times background fluorescence such as autofluorescent fat granules in the intestine (Fig. 2c). The target neurons are then distinguished from the background fluorescence based on a number of features such as relative distances between objects, position of the objects, and their sizes (Fig. 2d). The x-y-z stage then moves the device such that the two neurons are near the laser spot. A denser z-stack (0.5-μm step size) is subsequently obtained and processed to identify x-y-z coordinates of center of each neuron. The program then moves the stage to center on the target neuron (Fig. 2e) and triggers the laser firing. We used a 5 mM coumarin 120 (7-amino-4-methylcoumarin) dye laser excited by a VSL-337ND-S laser (Spectra-physics).[5] This dye laser produces 3 ns pulses with a wavelength of 440 nm. The laser is focused *via* the 100× (NA = 1.4) objective to a diffraction-limited spot, which is about the same as the wavelength of the laser.[5] Forty pulses are delivered at a pulse rate of 30 Hz. The intensity of the laser beam was adjusted by neutral density filters so that it was just possible to scratch the coverslip.[5] To verify the accuracy of the image processing and laser firing, worm images before (Fig. 2e, g) and after

laser firing (Fig. 2f, h) were saved. The entire cycle takes 15 seconds when we ablate two neurons, where the majority time is spent by the travel of the x-y-z stage. This automated cell-identification and laser firing process is an essential element of the microsystem to achieve high-throughput cell ablation with a high degree of accuracy and uniform treatment of the sample.

To demonstrate the capability of this system, we ablate animals with the olfactory neurons AWBL/R expressing *str-1-GFP*[13] at a sustained rate of 110 worms per hour to generate enough worms for a population behavior assay. Typically a population-based assay requires at least 50–100 age-synchronized worms per assay and multiple repeats.[14] The traditional manual laser ablation method cannot provide such a large number of animals, while genetically mediated cell disruption using cytotoxic genes does not necessarily eliminate the target neurons completely and efficiently and may complicate interpretation of behavior data.[7] For instance, animals expressing the degenerin gene *mec-4(d)* in AWB showed diminished avoidance, but it was unclear whether the residual avoidance is due to residual AWB function or to the contribution of other sensory neurons.[13] Here we ablate ~350 pairs of AWBL/R neurons to generate enough animals for the behavior assay.

In order to diminish the animals' ability to sense 2-nonanone significantly, both neurons have to be correctly ablated. Our image analysis algorithm can successfully distinguish the target cells from auto-fluorescent fat granules (Fig. 2 a-d) using anatomical information of the neurons (Fig. 3a and Supplementary Methods†). The cell-identification algorithm was 99% correct in targeting cells (348 pairs of neurons in 352 animals), verified by the images recorded for laser ablation. The success rate of the two-cell ablation was 89% (313 pairs of neurons in 352 animals). Successful ablation was confirmed by looking for *str-1-GFP* expression in AWBL/R 2 days after the ablation.[15] We performed 2-nonanone chemotaxis assays with populations of worms: the chemotaxis was measured by establishing a concentration gradient of the avoidant from a point source in a 10-cm agar plate and observing the final distribution of animals on the assay plate after 1 hr (Supplementary Methods†).[13] The avoidance index can vary between −1.0 (perfect attraction) and 1.0 (perfect repulsion);[6] zero indicates random choice (neither attraction nor repulsion). Compared to both the control group (*i.e.* those not handled in micro device and not ablated) and the mock-ablated group (*i.e.* those handled in micro device but without laser firing), AWB-ablated animals exhibited greatly diminished avoidance of the volatile repellent (Fig. 3b), confirming that AWB neurons contribute to avoidance of 2-nonanone. Residual 2-nonanone avoidance suggests that other sensory neurons may also detect this repellent. These results show that our system can be used to perform automated ablation to provide a large number of ablated animals for understanding neurons' roles in behavior. Using other cell-specific markers, it is easy to adapt the system to ablate other cells for large-scale systematic studies in many other contexts, such as in development; this system can also be coupled with other lasers to perform, for example, laser surgery on subcellular structures. Moreover, we believe this system could be used as a high-resolution imaging tool for *C. elegans* in L1 stage to study its early development, such as synaptic remodeling and axon guidance.

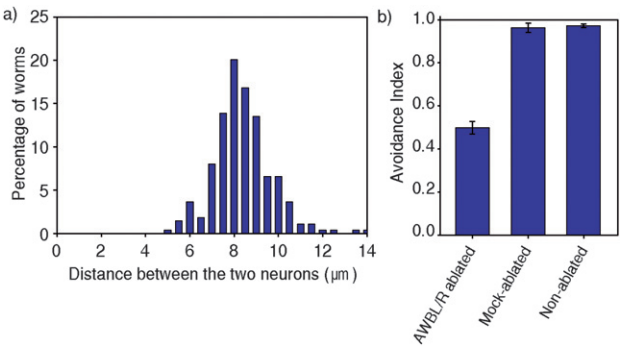

Fig. 3 a) Calculated distance between the two neurons of ablated worms by the image processing algorithm. Internal anatomical information of cells including relative distance was used to distinguish the target neurons from auto-fluorescent fat granules. b) 2-nonanone chemotaxis response of AWBL/R-ablated, mock-ablated, and control animals. AWBL/R ablated worms have defects in 2-nonanone avoidance behaviour. Each data point represents the average of at least five independent assays. Error bars indicate the standard error of the mean (SEM).

Acknowledgements

The authors acknowledge the US National Science Foundation (DBI-0149833) and the National Institutes of Health (NS058465) for funding. HL is a DuPong Young Professor and a Sloan Research Fellow in neuroscience.

Notes and references

1 J. E. Kimble and J. G. White, *Dev. Biol.*, 1981, **81**, 208–219.
2 M. Chalfie, J. E. Sulston, J. G. White, E. Southgate, J. N. Thomson and S. Brenner, *J. Neurosci.*, 1985, **5**, 956–964.
3 L. Avery and R. Horvitz, *Neuron*, 1989, **3**, 473–485.
4 M. Chalfie, Y. Tu, G. Euskirchen, W. W. Ward and D. C. Prasher, *Science*, 1994, **263**, 802–805.
5 C. I. Bargmann and L. Avery, in *Methods in Cell Biology*, 1995, pp. 225–250.
6 C. I. Bargmann, E. Hartwieg and H. R. Horvitz, *Cell*, 1993, **74**, 515–527.
7 S. Harbinder, N. Tavernarakis, L. A. Herndon, M. Kinnell, S. Q. Xu, A. Fire and M. Driscoll, *Proc. Natl. Acad. Sci. U. S. A.*, 1997, **94**, 13128–13133.
8 S. E. Hulme, S. S. Shevkoplyas, J. Apfeld, W. Fontana and G. M. Whitesides, *Lab Chip*, 2007, **7**, 1515–1523.
9 S. X. Guo, F. Bourgeois, T. Chokshi, N. J. Durr, M. A. Hilliard, N. Chronis and A. Ben-Yakar, *Nat. Methods*, 2008, **5**, 531–533.
10 F. Zeng, C. B. Rohde and M. F. Yanik, *Lab Chip*, 2008, **8**, 653–656.
11 K. Chung, M. M. Crane and H. Lu, *Nat. Methods*, 2008, **5**, 637–643.
12 T. V. Chokshi, A. Ben-Yakar and N. Chronis, *Lab Chip*, 2009, **9**, 151–157.
13 E. R. Troemel, B. E. Kimmel and C. I. Bargmann, *Cell*, 1997, **91**, 161–169.
14 A. C. Hart, ed., in *WormBook*, The *C. elegans* Research Community, 2006.
15 P. D. Wes and C. I. Bargmann, *Nature*, 2001, **410**, 698–701.

